A&A 467, L29–L32 (2007)
DOI: 10.1051/0004-6361:20077250

Astronomy & Astrophysics

Letter to the Editor

White dwarf masses derived from planetary nebula modelling⋆

K. Gesicki[1] and A. A. Zijlstra[2]

[1] Centrum Astronomii UMK, ul. Gagarina 11, 87-100 Torun, Poland
e-mail: Krzysztof.Gesicki@astri.uni.torun.pl
[2] School of Physics and Astronomy, University of Manchester, PO Box 88, Manchester M60 1QD, UK
e-mail: a.zijlstra@manchester.ac.uk

Received 7 February 2007 / Accepted 15 March 2007

ABSTRACT

Aims. We compare the mass distribution of central stars of planetary nebulae (CSPNe) with those of their progeny, white dwarfs (WD).
Methods. We use a dynamical method to measure masses with an uncertainty of 0.02 $M_{\odot}$.
Results. The CSPN mass distribution is sharply peaked at 0.61 $M_{\odot}$. The WD distribution peaks at lower masses (0.58 $M_{\odot}$) and shows a much broader range of masses. Some of the difference can be explained if the early post-AGB evolution is faster than predicted by the Blöcker tracks. Between 30 and 50 per cent of WD may avoid the PN phase because they have too low a mass. However, the discrepancy cannot be fully resolved and WD mass distributions may have been broadened by observational or model uncertainties.

Key words. planetary nebulae: general – stars: evolution – stars: white dwarfs

1. Introduction

White Dwarf (WD) mass distributions have been determined using a variety of different methods. Discrepancies exist between the different determinations in particular between the photometric and spectroscopic WD masses. Boudreault & Bergeron (2005) compared the masses derived by fitting the observed Balmer lines with masses derived from trigonometric parallaxes and photometry. They found differences of ∼50 per cent for cool (6500–14 000 K) DA white dwarfs. Spectroscopic masses are believed to be more accurate, especially for WDs in the temperature range between 15 000 and 40 000 K (Liebert et al. 2005). Atmospheric models are less well established for stars outside this range. For hotter WDs the atmospheric structure is modified by an (often unknown) amount of metals and by non-LTE effects. For cooler WDs convection has to be considered and the models are sensitive to the mixing length and the amount of helium convected to the surface (Boudreault & Bergeron 2005).

Central stars of planetary nebulae (CSPNe) provide a way to test the mass distributions. CSPNe evolve directly into WDs, with only very minor mass changes, allowing one to measure masses of currently forming white dwarfs. However, CSPN mass distributions have also been uncertain. For example, Napiwotzki (2006) shows that the very high CSPN masses (close to the Chandrasekhar limit) derived spectroscopically with state-of-the-art model atmospheres by Pauldrach et al. (2004) are physically implausible and masses close to the peak of the CSPN/WD mass distribution are more likely.

CSPN masses are normally obtained from the luminosities. But more accurate masses can be derived using the age-temperature diagram, obtainable from the surrounding planetary nebula (PN). Gesicki et al. (2006) applied this to a sample of 101 PNe. In this Letter we discuss the resulting mass distributions for hydrogen-rich and hydrogen-poor CSPNe and compare them with published WD masses.

2. Methods and results

2.1. Models

The method requires the age of the nebula and the temperature of the central star to be determined. Together these provide the heating time scale for the star.

We derive the age of the PNe using a combination of line ratios, diameters (taken from the literature), and new high resolution spectra (Gesicki et al. 2006). The diameters and line ratios are used to fit a spherically symmetric photo-ionization model. The model assumes a density distribution and finds a stellar black-body temperature. For each ion, the model finds a radial emissivity distribution. The observed line profiles for each ion represent the convolution of the thermal broadening and the expansion velocity at each radius. Thus, the line profiles for different ions are used to fit a velocity field. An iterative procedure is used to improve the ionization model. The emissivity distributions of different ions overlap, and this gives a strong constraint on the shape of the wings of the line profiles. A genetic algorithm, PIKAIA, is used to arrive at the optimum solution for ionization model and velocity field. A turbulent component is added if needed: turbulence is indicated by a Gaussian shape of the line profiles. The expansion velocities are found to increase with radius, due to the overpressure of the ionized region.

From the velocity field $v(r)$, we derive the mass-weighted average over the nebula, $v_{\rm av}$. This parameter has been shown to be robust against the simplifications. Different models which provide comparable quality fits give the same $v_{\rm av}$ to within 2 km s^{-1} (Gesicki et al. 2006). Applying this to a radius of 0.8 times the outer radius (equivalent to the mass-averaged radius) allows us to assign a kinematic age t to the nebula. A linear acceleration

⋆ Data is only available in electronic form at
http://www.aanda.org

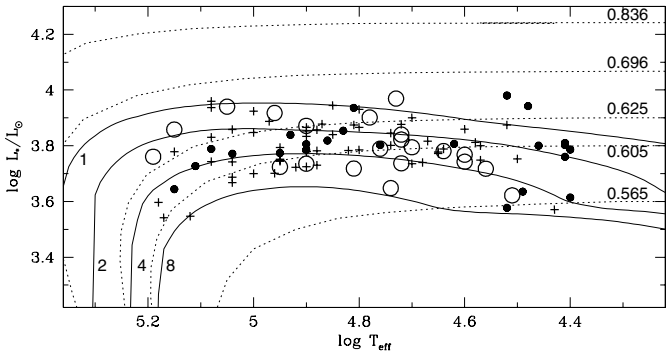

Fig. 1. Comparison of the 101 modelled PNe with the evolutionary tracks in the HR diagram. The model black-body temperatures are plotted against the luminosities interpolated from tracks. Filled circles indicate [WR] stars, open circles are *wels* and pluses indicate non-emission-line stars. The dotted lines show H-burning evolutionary models of Blöcker (1995), labeled by mass in units of $M_\odot$. The solid lines are isochrones, labeled by the time after the nebula ejection, in units of 10^3 yr.

is assumed to have occurred from the AGB expansion velocity (10–15 km s^{-1}) to the PN velocity $v_{\rm av}$ (20–25 km s^{-1}).

The derived nebular age and stellar temperature are compared to the the H-burning tracks of Blöcker (1995), which provide the largest and most uniform collection available. We interpolate between different tracks to find for each (t, $T_{\rm eff}$), the CSPN luminosity and mass.

2.2. Different CSPN types

The CSPNe fall into two broad categories: the hydrogen-rich O-type stars and the emission-line central stars which are generally hydrogen-deficient. The second group consists of [WR]-type stars with strong emission lines and *wels* (weak emission line stars). The [WR] are subdivided into hot [WO] and cool [WC]. [WR] stars are in most cases hydrogen-free (three possible exceptions are mentioned by Werner & Herwig 2006). The *wels* may contain some hydrogen. Gesicki et al. (2006) show that one group of *wels* is located in the temperature gap between [WC] and [WO] stars. The other *wels* stars form a non-uniform group, including higher-mass objects where the high luminosity drives a wind but the star is not necessarily hydrogen-poor. The hydrogen-rich stars are believed to be related to the DA white dwarfs, while the [WR] may evolved into DB's.

2.3. The HR diagram

The full analyzed sample contains 101 PNe, of which about 60 are in the direction of the Galactic Bulge and the remainder are in the Galactic disk. Foreground confusion among the Bulge PNe is estimated at 20%. The sample contains 23 [WR]-type, 21 *wels* and 57 non-emission-line central stars[1]. The CSPN classification was adopted from the literature. The last group contains also objects without any information about their spectrum.

In Fig. 1 we show the photoionization temperatures and interpolated luminosities, plotted on the HR diagram. The H-burning tracks of Blöcker (1995) are also shown: the luminosities and masses of CSPNe fall into a rather restricted range of values. Isochrones of 1, 2, 4, and 8×10^3 yr are also shown.

[1] The data file is only available in electronic form.

Table 1. Comparison between our dynamical masses and spectroscopic masses from Kudritzki et al. (2006). Observed mass-loss rates from the same paper are also listed and compared to values from the model tracks of Blöcker (1995). He 2-108 is classified as *wels*, the other three are non-emission-line stars.

Object	M [$M_\odot$]		$T_{\rm eff}$ [10^3 K]		log $\dot{M}$ [$M_\odot$ yr^{-1}]	
	dyn.	spec.	dyn.	spec.	spec.	evol. tracks
Tc 1	0.59	0.81	32	34	−7.46	−7.91
He 2-108	0.57	0.63	32	34	−6.85	−8.16
IC 418	0.61	0.92	37	36	−7.43	−7.82
NGC 3242	0.61	0.63	79	75	−8.08	−7.86

A previous HR diagram of CSPNe presented by Stanghellini et al. (2002) shows a much broader range of luminosities and, in consequence, masses. They use Zanstra temperatures and luminosities. The Zanstra method of locating a CSPN in the HR diagram was criticized by Schönberner & Tylenda (1990). Observationally, the accuracy of the luminosity determinations is about a factor of 2. On the Schönberner tracks, a CSPN mass change from, e.g., 0.57 to 0.7 $M_\odot$ corresponds to a factor of 3 in luminosity. The masses determined directly from luminosities are thus accurate to only 0.1 $M_\odot$. This is less than the typical dispersion of masses. In contrast, for the same mass range, the dynamical time scales differ by a factor of 60. Even for a factor of 2 uncertainty in the nebular age, the mass changes by only 0.02 $M_\odot$. Therefore, the dynamical method improves the accuracy.

Schönberner & Tylenda (1990) also developed a method to improve the CSPN mass determination. This method (Tylenda et al. 1991) results in masses similar to ours.

Table 1 compares, for four objects in common, our dynamical masses with the spectroscopic masses derived by Kudritzki et al. (2006). The spectroscopic masses are larger, in two cases very much larger. The lower masses are supported by the kinematical properties of Tc 1 and He 2-108 (see Fig. 5 of Napiwotzki 2006), which favour an old thin disk population. Kudritzki et al. also derive $T_{\rm eff}$: our photo-ionization values are in good agreement.

Pauldrach et al. (2004) find from a spectroscopic analysis, five CSPNe with masses close to the Chandrasekhar limit. This result is implausible, as argued by Napiwotzki (2006). Three of their objects are also in our sample, and all are found to have regular masses.

2.4. The mass distributions

In Fig. 2 the upper panel presents the mass distribution of our whole sample of 101 PNe. All CSPNe masses fall into a narrow range, 0.55–0.66 $M_\odot$, with a mean mass of 0.61 $M_\odot$. The range of masses is almost identical to that of Tylenda et al. (1991) but they obtained a smaller mean mass of 0.593 $M_\odot$ and their distribution peaks at 0.58 $M_\odot$.

The lower panel of Fig. 2 presents masses for the same types of CSPNe as shown in Fig. 1. The non-emission-line stars show a Gaussian mass distribution. The hydrogen-deficient emission-line stars seem to consist of two populations: one sharply peaked, containing [WR] stars, and the other showing a wider spread, composed of [WR] and *wels*. The sharp peak consists, with a single exception, of hot [WO] stars only.

The presented histograms seem to suggest that hot [WO] stars form a different group from the combined cooler [WC] and *wels* CSPNe.

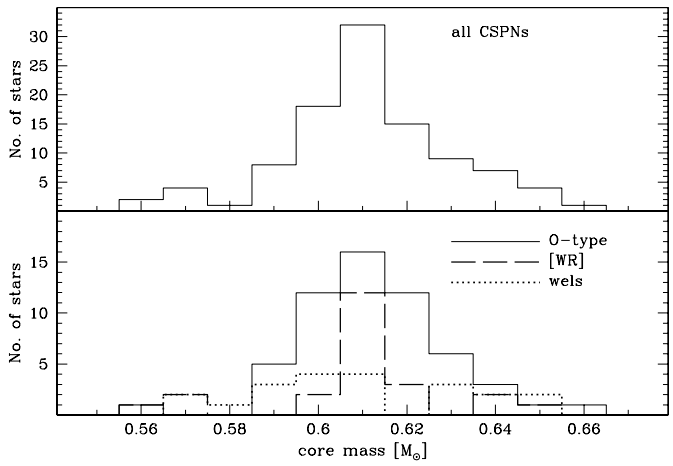

Fig. 2. The CSPN mass histograms. *Upper panel*: the histogram of all modelled PNe. *Lower panel*: the histogram of different subgroups of the 101 PNe. The dashed line indicates [WR] stars, the dotted line *wels* and the solid line non-emission-line stars.

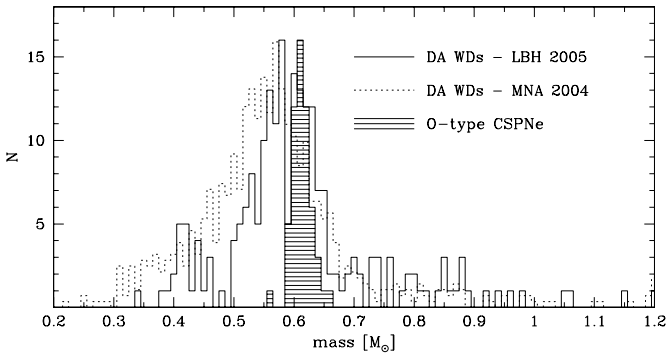

Fig. 3. The mass distribution of non-emission-line O-type CSPNe (shaded area) is compared to two DA white dwarf distributions of intermediate temperatures: thin line: data from Liebert et al. (2005); dotted line: data from Madej et al. (2004) which are more numerous, and are rescaled.

3. Comparing CSPNe and WDs

3.1. The histograms

The comparable birth rates of PNe and WDs suggests that most white dwarfs go through the PN phase (e.g. Liebert et al. 2005). The two mass distribution should therefore be similar.

Figure 3 presents the histograms of our interpolated O-type CSPN masses and the masses of DA white dwarfs from recent surveys. The WD data of Madej et al. (2004), kindly provided by the authors, contain 1175 new DA WDs extracted from the Sloan Digital Sky Survey. The data of Liebert et al. (2005), taken from the electronic version of their article, contain 347 DA WDs from the Palomar Green Survey. For Fig. 3 we selected the objects with temperatures between 15 000 K and 40 000 K. The two WDs histograms are not identical, but both peak at similar values and show extended low- and high-mass tails. We plot the histograms using narrower bins than usually done for WDs, optimized to the mass resolution of our CSPN data. The difference between the WD and CSPN distributions is striking.

First, the obtained CSPN masses are restricted to a much narrower range of values than WDs, and are also much more sharply peaked. At face value, this implies that only some of the WDs have gone through the PN phase, in contrast to the conclusion from their similar birth rates (Liebert et al. 2005). Second, the two distributions peak at different masses. Here a systematic error cannot be excluded, as discussed below.

3.2. Hydrogen-rich vs. hydrogen-deficient

Hansen & Liebert (2003) point to a variety of WD mass distributions with clear differences between hydrogen- and helium-rich cool stars. Beauchamp et al. (1996) found for hot helium-atmosphere DB stars a sharp peak and an almost complete lack of low- and high-mass components. They also found that the DBA stars, which exhibit traces of atmospheric hydrogen, show a distinctly different, broad and flat distribution.

The CSPN show an apparent difference between hydrogen-rich and hydrogen-deficient mass distributions. The hydrogen-deficient stars show a very narrow mass distribution; it is tempting to relate this to the helium-rich DB and DBA populations. We use hydrogen-burning tracks to derive these masses. The evolution after the thermal pulse leading to helium burners is very complicated and not well understood (Werner & Herwig 2006). This may not affect the derived masses too much: the effect of a thermal pulse is to change the temperature of the star, but as shown in Fig. 1, the isochrones have only a weak dependence on temperature. The resulting offset in time (still very uncertain), when accounted for, can shift those CSPN masses towards higher values.

4. Discussion

4.1. Uncertainties in mass determinations

When comparing the CSPNe and WDs we have to remember that we compare different spatial distributions. Because of their faintness the WD observations are restricted to our nearest neighbourhood while PNe are observed across the whole Galaxy. Nevertheless we did not obtain significantly different distributions for PNe at different distances.

Our mass determination relies on a single set of evolutionary tracks. There are two possible sources of error in the Blöcker tracks. The first is the early post-AGB evolution where the time scales depend on how and when the AGB wind terminates. The Blöcker tracks end this at $T_{\rm eff} \sim 6000$ K, (pulsation period of 50 days) to agree with the observations of detached shells around hotter stars but not around cooler stars. A later termination would lead to an earlier start of the ionization: in this case we would systematically overestimate the masses. For a reduction of the post-AGB transition time by 10^3 yr, the typical mass would reduce by 0.01 $M_\odot$.

The second uncertainty is the mass-loss rate during the post-AGB phase. For $M \sim 0.6\ M_\odot$, the post-AGB mass-loss rate in the Blöcker models is 0.1 times the nuclear burning rate, but for high-mass models the mass loss accelerates the evolution by 50% (Blöcker 1995). A higher post-AGB mass loss than assumed would reduce our masses, but for the typical masses we find a very large increase would be required. Table 1 compares the Blöcker mass-loss rates with observed values, where we used the dynamical mass to calculate the Blöcker rate. For the three non-emission-line stars, observed rates are higher by up to a factor of 3. This appears to be in part related to the high luminosity derived by Kudritzki et al.: if we compare their rates with Blöcker tracks at similar luminosity, then the Blöcker rates tend to be higher. The nuclear burning rate of $\dot{M}_{\rm H} \sim -6.8$ exceeds the observed wind mass-loss rate by a factor of four (more for NGC 3242). For this factor, the Blöcker tracks would

Table 2. Blöcker track time scales: PN visibility is defined as between $\log T_{\rm eff} = 4.4$ and either a nebular age $t = 10^4$ yr or a stellar luminosity $\log L = 3.0$, whichever occurs earlier.

Mass [$M_\odot$]	$t_{\rm start}$ [yr]	$t_{\rm end}$ [yr]	$t_{\rm visibility}$ [yr]
0.546	90×10^3	–	–
0.565	4×10^3	10×10^3	6×10^3
0.605	1.5×10^3	7.4×10^3	5.9×10^3
0.625	660	3.6×10^3	2.9×10^3
0.696	100	880	780
0.836	100	840	740
0.940	12	90	78

underestimate the speed of evolution by only 10 per cent. We conclude that the post-AGB mass-loss rates have little effect on the derived masses. The exception is the *wels* in the sample, where the wind mass loss rate is comparable to the nuclear burning rate.

There is also an uncertainty in the dynamical age estimate. A later acceleration would increase the ages by up to 50 per cent and shift the mass peak from 0.61 to 0.60 $M_\odot$.

The WD mass determinations also suffer from simplifications and model assumptions, in addition to the uncertainties concerning cool and hot WDs as described in the Introduction. One uncertainty is in contemporary plasma physics, concerning the pressure broadening in a very high density plasma (Madej et al. 2004). The mass-radius relations used depend on the assumed mass of the hydrogen layer. Napiwotzki et al. (1999) compared estimates from different studies and concluded that the gravities obtained from the spectroscopic method suffer from systematic errors of up to 0.1 dex in $\log g$. This corresponds to an offset in masses of about 0.02 $M_\odot$ and could, in principle, explain the difference in peak masses between WDs and CSPNe. The width of the peak may also be narrower than derived from the models. Nevertheless, the wide tails of the mass distribution are not in doubt.

4.2. Time scales, birth rates and binarity

The derived CSPN mass distribution combines the effects of the birth rate as a function of mass, and the observable life time of the PN. The latter depends on mass as indicated in Table 2. The period of visibility is defined here as beginning when the star reaches $T_{\rm eff} = 25 \times 10^3$ K, and ending either when the star enters the cooling track (defined as $\log L = 3.00$) or when the age of the nebula is 10^4 yr, whichever comes earlier. Our histogram should be corrected for the difference in visibility time. This increases the number at high CSPN mass only by a factor of up to 10, and brings the high mass tail into somewhat better agreement. We may also have a sample bias against high masses, as these are not expected in the Bulge objects. The de-selection of bipolar objects may have removed a few higher-mass nebulae in the disk.

CSPNe with $M < 0.56\ M_\odot$ would not produce a visible PN, as the post-AGB transition time becomes too long ("lazy PNe"). In the sample of Liebert et al. (2005), 30 per cent of white dwarfs have masses in this range, and 50 per cent in the sample of Madej et al. (2004). However, the sharp drop in the CSPN mass distribution below 0.60 $M_\odot$ occurs at too high a mass to be affected.

Hansen & Liebert (2003) argue that both the high- and low-mass tails in the WD distribution can be a result of binary evolution. Merging leads to high-mass WDs while a close companion stripping the envelope can cause an early termination of the evolution and produce a low-mass helium WD. Both channels together may account for some 10 per cent of all WDs (Moe & de Marco 2006). Therefore the histogram for single WDs could be narrower. Close binary evolution can affect the PN phase as well, leading to strongly non-spherical nebulae. Our model analysis assumes spherical symmetry, and we did not analyze bipolar nebulae. Our selection therefore favours single CSPNe and rejects low-mass CSPNe in interacting binaries. Thus, the CSPN histogram (Fig. 3) is biased toward single-star evolution, while the WD histogram includes binary broadening. This may affect the tails of the WD histogram but is not expected to affect the main peak.

Moe & de Marco (2006) predict the number of PNe in the Galaxy to be around 46 000. Based on local column densities, Zijlstra & Pottasch (1991) derive an actual number of 23 000, suggesting that only about half the stars which could produce a PN, do so. This comparison is limited by our knowledge on the time a PN remains observable. Moe & de Marco (2006) predict a birth rate of PNe of 1.1×10^{-12} PNe yr^{-1} pc^{-3}, comparable to the current, local WD birth rate of 1.0×10^{-12} PNe yr^{-1} pc^{-3}. Again assuming only half their predicted number of PNe is actually observed, the expectation is that half of all WDs have passed through the PN phase.

5. Conclusions

We show that the mass distribution of CSPNe is sharply peaked at $M = 0.61\ M_\odot$. The published WD mass distributions show a much broader distribution peaking at a lower mass of $M = 0.59\ M_\odot$. Part of the difference in the peak may indicate faster evolution during the early post-AGB phase than assumed in the Blöcker tracks. CSPN mass-loss rates cannot explain the difference. However considering the uncertainty of 0.02 $M_\odot$ in the WD mass estimations both peaks are in reasonable agreement. About 30 per cent of WDs have too low a mass to have passed through the PN phase.

Acknowledgements. We thank our referee Ralf Napiwotzki for important comments. This project was financially supported by the "Polish State Committee for Scientific Research" through the grant No. 2.P03D.002.025 and by a NATO collaborative program grant No. PST.CLG.979726. A.A.Z. and K.G. gratefully acknowledge hospitality from the SAAO.

References

Beauchamp, A., Wesemael, F., & Bergeron, P. 1996, in Hydrogen-Deficient Stars, ed. C. S. Jeffery, & U. Heber, ASP Conf. Ser., 96, 295
Blöcker, T. 1995, A&A, 299, 755
Boudreault, S., & Bergeron, P. 2005, ASP Conf. Ser., 334, 249
Gesicki, K., Zijlstra, A. A., Acker, A., et al. 2006, A&A, 451, 925
Hansen, B. M. S., & Liebert, J. 2003, ARA&A, 41, 465
Kudritzki, R. P., Urbaneja, M. A., & Puls, J. 2006, Planetary Nebulae in our Galaxy and Beyond, ed. M. J. Barlow, & R. H. Méndez (CUP Cambridge), IAU Symp., 234, 119
Liebert, J., Bergeron, P., & Holberg, J. B. 2005, ApJS, 156, 47
Madej, J., Nalezyty, M., & Althaus, L. G. 2004, A&A, 419, L5
Moe, M., & de Marco, O. 2006, ApJ, 650, 916
Napiwotzki, R., Green, P. J., & Saffer, R. A. 1999, ApJ, 517, 399
Napiwotzki, R. 2006, A&A, 451, L27
Pauldrach, A. W. A., Hoffmann, T. L., & Mendez, R. H. 2004, A&A, 419, 1111
Schönberner, D., & Tylenda, R. 1990, A&A, 234, 439
Stanghellini, L., Villaver, E., Manchado, A., & Guerrero, M. A. 2002, ApJ, 576, 285
Tylenda, R., Stasińska, G., Acker, A., & Stenholm, B. 1991, A&A, 246, 221
Werner, K., & Herwig, F. 2006, PASP, 118, 183
Zijlstra, A. A., & Pottasch, S. R. 1991, A&A, 243, 478

Online Material

Table 3. The table contains the results collected over years of planetary nebulae modelling with Torun codes. First two columns identify the object. Next five columns contain the photoionization model parameters: logarithm of stellar black-body temperature, logarithm of stellar luminosity, assumed distance, nebular outer radius and ionized mass. Columns 8 and 9 contain the derived mass-averaged expansion velocity and turbulence. Columns 10 and 11 contain values interpolated from evolutionary tracks: stellar luminosity and its mass. Column 12 contains the derived kinematic age. Last column lists reference to the publication of data.

Object		Photoionization model parameters							Interpolated			
PN G	Name	$\log T_{\rm b-b}$	$\log L/L_\odot$	Dist.	$R_{\rm out}$	$M_{\rm ion}$	$v_{\rm av}$	$v_{\rm turb}$	$\log L/L_\odot$	$M_{\rm core}$	$t_{\rm kin}$	Ref.
		[K]		[kpc]	[pc]	$[M_\odot]$	[km s^{-1}]			$[M_\odot]$	10^3 yr	
000.9-04.8	M 3-23	5.18	3.0	4.0	0.11	0.10	24.	13	3.59623	0.61146	5.06180	8
001.5-06.7	SwSt 1	4.52	4.3	2.0	0.007	0.011	17.	14	3.98030	0.64994	0.40563	4
001.7-04.6	H 1-56	4.95	3.0	10.0	0.08	0.12	17.	0	3.74856	0.60471	4.63572	5
002.0-06.2	M 2-33	4.74	3.3	8.0	0.10	0.27	12.	0	3.64800	0.57455	7.11162	5
002.0-13.4	IC 4776	4.60	3.6	3.5	0.06	0.18	22.	0	3.76774	0.59872	2.93354	5
002.1-02.2	M 3-20	4.88	3.2	7.0	0.10	0.27	32.	0	3.78154	0.60751	3.72514	5
002.6-03.4	M 1-37	4.40	3.9	8.0	0.04	0.08	27.	0	3.78642	0.60237	1.69141	8
002.6+08.1	H 1-11	4.81	3.4	7.0	0.10	0.21	19.	0	3.71811	0.59068	5.39502	6
002.7-04.8	M 1-42	4.92	3.0	4.0	0.08	0.16	13.	0	3.72295	0.59784	5.44194	8
003.1+02.9	Hb 4	4.95	3.6	4.0	0.065	0.2	16.	14	3.77384	0.60902	3.91139	4
003.2-06.2	M 2-36	4.90	3.3	6.4	0.11	0.38	22.	0	3.72494	0.59708	5.37816	5
003.6+03.1	M 2-14	4.64	3.0	8.0	0.05	0.06	17.	10	3.78088	0.60231	2.89733	8
003.7-04.6	M 2-30	5.04	3.5	7.0	0.10	0.36	26.	0	3.74235	0.60977	4.34599	5
003.8-17.1	Hb 8	4.88	3.4	15.0	0.04	0.09	22.	0	3.85697	0.62160	1.95570	5
003.9-02.3	M 1-35	4.85	3.6	4.5	0.05	0.138	25.	0	3.84039	0.61749	2.23508	6
004.0-03.0	M 2-29	4.88	3.3	9.0	0.08	0.23	14.	0	3.72973	0.59704	5.21519	5
004.2-04.3	H 1-60	4.90	3.0	7.0	0.10	0.21	21.	0	3.73553	0.59949	5.04696	5
004.6+06.0	H 1-24	4.56	3.8	7.0	0.08	0.13	24.	0	3.71760	0.58483	3.68131	8
004.9+04.9	M 1-25	4.62	3.8	8.0	0.06	0.18	30.	12	3.80650	0.60733	2.34684	4
005.2+05.6	M 3-12	5.0	3.2	8.0	0.15	0.57	30.	0	3.69984	0.59962	5.86709	4
005.8-06.1	NGC 6620	5.04	3.3	8.0	0.14	0.45	27.	0	3.68710	0.60138	5.91995	4
006.0-03.6	M 2-31	4.86	3.7	8.0	0.07	0.26	30.	15	3.81865	0.61364	2.73797	7
006.1+08.3	M 1-20	4.90	3.4	6.0	0.026	0.045	12.	0	3.86600	0.62411	1.84902	6
006.4+02.0	M 1-31	4.76	3.8	8.0	0.06	0.29	19.	0	3.78944	0.60587	3.23701	8
006.8+04.1	M 3-15	4.90	3.6	4.0	0.06	0.19	16.	15	3.78549	0.60904	3.61052	4
008.2+06.8	He 2-260	4.80	3.2	12.0	0.06	0.13	17.	0	3.78478	0.60585	3.47679	8
008.3-01.1	M 1-40	5.15	3.3	2.5	0.042	0.067	27.	0	3.85805	0.64136	1.77598	4
009.4-09.8	M 3-32	4.95	3.2	7.0	0.10	0.26	23.	0	3.74476	0.60407	4.74108	5
009.6-10.6	M 3-33	4.95	3.3	8.0	0.12	0.40	25.	0	3.72404	0.60009	5.36420	5
010.7-06.4	IC 4732	4.82	3.6	8.0	0.08	0.29	25.	0	3.78307	0.60601	3.57613	5
027.6+04.2	M 2-43	4.81	3.6	5.0	0.02	0.039	20.	10	3.93608	0.63867	1.04304	4
029.2-05.9	NGC 6751	4.90	3.0	2.0	0.1	0.15	41.	15	3.80594	0.61265	3.06776	4
064.7+05.0	BD+30	4.41	4.1	2.6	0.035	0.08	27.	15	3.81013	0.60724	1.47999	4
096.4+29.9	NGC 6543	4.70	3.6	1.1	0.05	0.12	17.	12	3.79443	0.60585	2.89733	4
120.0+09.8	NGC 40	4.52	3.3	1.2	0.14	0.25	25.	8	3.57745	0.56427	6.25823	4
123.6+34.5	IC 3568	4.68	3.9	2.0	0.1	0.13	29.	0	3.74033	0.59264	4.01168	4
144.5+06.5	NGC 1501	5.15	3.8	1.2	0.16	0.18	40.	10	3.64436	0.61050	5.00658	4
146.7+07.6	M 4-18	4.4	3.8	6.8	0.06	0.1	15.	15	3.61432	0.56699	3.75494	4
211.2-03.5	M 1-6	4.60	3.5	4.0	0.03	0.05	24.	0	3.85947	0.61760	1.38049	8
215.2-24.2	IC 418	4.57	3.9	1.0	0.036	0.05	15.	0	3.79977	0.60566	2.25296	4
217.4+02.0	St 3-1	4.96	2.5	4.0	0.14	0.20	26.	0	3.70056	0.59589	6.08439	8
221.3-12.3	IC 2165	5.19	3.2	2.5	0.057	0.076	25.	14	3.76072	0.63015	2.54799	4
232.0+05.7	SaSt 2-3	4.80	2.5	4.0	0.02	0.01	19.	0	3.93049	0.63679	1.07900	8
232.4-01.8	M 1-13	5.04	2.9	4.0	0.10	0.19	14.	0	3.66755	0.59792	6.51899	8
253.9+05.7	M 3-6	4.72	4.0	1.5	0.036	0.03	18.	0	3.83991	0.61485	2.01157	8
258.1-00.3	He 2-9	4.73	2.9	1.5	0.015	0.01	25.	0	3.96926	0.64835	0.67052	8
261.0+32.0	NGC 3242	4.9	3.3	1.0	0.1	0.15	31.	0	3.77838	0.60772	3.81599	4
261.6+03.0	He 2-15	5.17	3.0	2.2	0.13	0.32	22.	0	3.54221	0.60566	6.35601	8
278.1-05.9	NGC 2867	5.08	3.1	2.0	0.07	0.15	28.	12	3.78876	0.62018	2.88208	6
278.8+04.9	PB 6	5.04	2.7	4.0	0.1	0.18	34.	16	3.77138	0.61423	3.55581	6
283.3+03.9	He 2-50	5.12	2.9	5.1	0.14	0.32	17.	0	3.54669	0.59451	8.11252	8
285.4+01.5	Pe 1-1	4.93	3.3	3.5	0.05	0.038	24.	10	3.83898	0.61981	2.30082	4
292.4+04.1	PB 8	4.76	3.6	5.0	0.06	0.18	22.	09	3.80234	0.60832	2.93354	8
296.3-03.0	He 2-73	5.00	3.7	4.0	0.04	0.11	19.	0	3.84716	0.62464	2.15801	5

Table 3. continued.

Object		Photoionization model parameters							Interpolated			
PN G	Name	$\log T_{\rm b-b}$	$\log L/L_\odot$	Dist.	$R_{\rm out}$	$M_{\rm ion}$	$v_{\rm av}$	$v_{\rm turb}$	$\log L/L_\odot$	$M_{\rm core}$	$t_{\rm kin}$	Ref.
		[K]		[kpc]	[pc]	[$M_\odot$]	[km s^{-1}]			[$M_\odot$]	10^3 yr	
300.7-02.0	He 2-86	4.83	3.4	3.0	0.03	0.05	14.	11	3.85377	0.61958	1.95570	8
304.8+05.1	He 2-88	4.72	2.8	4.0	0.03	0.03	23.	0	3.87629	0.62213	1.42232	8
307.2-09.0	He 2-97	4.81	3.3	4.5	0.03	0.05	19.	0	3.87420	0.62326	1.61851	5
309.0-04.2	He 2-99	4.49	2.7	4.0	0.16	0.25	45.	10	3.63538	0.57008	4.55144	8
316.1+08.4	He 2-108	4.51	3.8	4.0	0.10	0.14	21.	09	3.62192	0.56865	5.04696	8
321.0+03.9	He 2-113	4.48	2.8	2.0	0.01	0.003	18.	15	3.94205	0.63638	0.55877	8
325.0+03.2	He 2-129	4.87	3.8	7.0	0.03	0.08	18.	13	3.87817	0.62570	1.67631	8
325.8+04.5	He 2-128	4.70	3.3	5.0	0.06	0.13	12.	10	3.73533	0.59173	4.26697	8
327.1-02.2	He 2-142	4.41	3.7	3.5	0.03	0.03	20.	7	3.80232	0.60571	1.56456	4
327.5+13.3	He 2-118	4.90	3.0	7.0	0.03	0.03	13.	0	3.85268	0.62141	2.04073	5
345.0-04.9	Cn 1-3	4.65	3.6	7.5	0.05	0.12	16.	0	3.77769	0.60171	3.00876	5
345.2-08.8	Tc 1	4.5	3.5	2.0	0.05	0.05	20.	0	3.75304	0.59402	2.60759	4
346.3-06.8	Fg 2	5.08	3.2	8.7	0.10	0.22	30.	0	3.74337	0.61349	3.91139	5
347.4+05.8	H 1-2	4.96	3.9	7.0	0.02	0.06	13.	10	3.91769	0.63917	1.36048	8
349.8+04.4	M 2-4	4.74	3.8	6.0	0.05	0.16	17.	0	3.80114	0.60774	2.89733	5
350.9+04.4	H 2-1	4.52	3.9	5.0	0.03	0.06	36.	0	3.87450	0.62022	1.02036	5
351.1+04.8	M 1-19	4.72	3.2	11.0	0.10	0.20	26.	0	3.73705	0.59269	4.34599	8
351.9+09.0	PC 13	4.95	3.9	6.0	0.10	0.15	29.	0	3.77032	0.60842	4.01168	5
352.1+05.1	M 2-8	5.11	3.2	7.0	0.06	0.16	14.	14	3.72721	0.61451	3.91139	8
352.9-07.5	Fg 3	4.67	4.0	7.0	0.03	0.09	10.	0	3.81592	0.60964	2.34684	5
352.9+11.4	K 2-16	4.46	3.3	1.0	0.05	0.002	34.	12	3.80036	0.60541	1.77791	4
353.3+06.3	M 2-6	4.74	3.7	8.4	0.04	0.103	22.	0	3.84523	0.61616	1.95570	6
353.5-04.9	H 1-36	5.08	3.5	7.0	0.03	0.061	32.	0	3.93679	0.65433	1.11754	6
355.1-06.9	M 3-21	4.95	3.2	5.0	0.06	0.11	18.	0	3.85873	0.62963	2.01878	5
355.1-02.9	H 1-31	5.04	3.7	12.0	0.04	0.11	21.	0	3.79399	0.61248	3.35262	5
355.4-02.4	M 3-14	4.90	3.8	6.0	0.08	0.35	23.	0	3.77925	0.60787	3.79287	5
355.7-03.5	H 1-35	4.65	4.0	8.0	0.04	0.14	10.	0	3.77165	0.60030	3.12911	5
355.9-04.2	M 1-30	4.60	3.8	8.0	0.07	0.22	22.	0	3.74277	0.59194	3.42247	4
355.9+03.6	H 1-9	4.58	4.0	9.0	0.04	0.09	20.	0	3.81243	0.60821	2.08608	8
356.1+02.7	Th 3-13	5.05	3.3	8.0	0.03	0.05	32.	0	3.94019	0.65232	1.11754	8
356.2-04.4	Cn 2-1	4.90	3.6	6.0	0.04	0.087	25.	0	3.87156	0.62528	1.78807	6
356.5-02.3	M 1-27	4.41	3.6	3.0	0.04	0.05	21.	0	3.76041	0.59577	2.01878	8
356.9+04.5	M 2-11	5.15	2.7	7.0	0.05	0.06	20.	0	3.77884	0.62664	2.60759	5
357.1+03.6	M 3-7	4.72	3.2	4.0	0.05	0.07	23.	0	3.82222	0.61146	2.37054	8
357.2+07.4	M 4-3	4.80	3.6	8.0	0.033	0.075	20.	0	3.86542	0.62123	1.72101	6
357.4-03.5	M 2-18	4.64	3.5	7.0	0.06	0.09	24.	0	3.75162	0.60526	4.54226	8
357.4-03.2	M 2-16	4.95	3.3	7.0	0.09	0.25	21.	14	3.78822	0.60388	2.76098	8
358.2+03.6	M 3-10	4.97	3.0	5.0	0.04	0.048	27.	0	3.88764	0.63182	1.69141	6
358.5-04.2	H 1-46	4.70	3.9	7.0	0.02	0.045	17.	0	3.90050	0.62728	1.15893	6
358.7-05.2	M 3-40	5.00	3.3	7.6	0.03	0.05	26.	0	3.92420	0.64333	1.30380	5
359.1-02.3	M 3-16	4.57	3.8	7.0	0.08	0.14	30.	0	3.74833	0.59317	3.12911	8
359.1-01.7	M 1-29	5.08	3.5	3.0	0.05	0.128	24.	0	3.82983	0.62709	2.30082	6
359.2-33.5	CRBB 1	4.43	3.8	3.5	0.08	0.18	13.	0	3.57111	0.56316	5.44194	4
359.3-00.9	Hb 5	5.08	3.5	1.3	0.02	0.03	25.	0	3.95924	0.66284	0.89403	5
359.7-02.6	H 1-40	4.85	3.6	7.80	0.02	0.04	21.	0	3.94494	0.64258	1.00939	5
359.8-07.2	M 2-32	4.90	3.6	7.00	0.06	0.19	29.	0	3.83374	0.61773	2.40701	5
359.9-04.5	M 2-27	4.78	3.7	5.50	0.03	0.069	26.	0	3.90137	0.62872	1.30380	6

References:

4: Acker et al. 2002, A&A 384, 620.
5: Gesicki & Zijlstra 2000, A&A 358, 1058.
6: Gesicki et al. 2003, A&A 400, 957.
7: Gesicki & Zijlstra 2003, MNRAS 338, 347.
8: Gesicki et al. 2006, A&A 451, 925.